Journal of Nuclear Medicine, published on March 3, 2016 as doi:10.2967/jnumed.115.169839

Molecular Imaging and Quantitation of EphA2 Expression in Xenograft Models with ^{89}Zr-DS-8895a

Ingrid J.G. Burvenich[1,2*], Sagun Parakh[1,2,3*] , Hui K. Gan[1,2,3], Fook-Thean Lee[1], Nancy Guo[1], Angela Rigopoulos[1], Sze-Ting Lee[1,4], Sylvia Gong[4], Graeme J. O'Keefe[3,4], Henri Tochon-Danguy[4], Masakatsu Kotsuma[5], Jun Hasegawa[6], Giorgio Senaldi[7] and Andrew M. Scott[1,3,4,8]

[1]Tumour Targeting Laboratory, Ludwig Institute for Cancer Research and Olivia Newton-John Cancer Research Institute, Melbourne, Australia

[2]School of Cancer Medicine, La Trobe University, Melbourne, Australia

[3]Department of Medical Oncology, Austin Health, Heidelberg, Melbourne, Australia;

[4]Departmentof Molecular Imaging and Therapy, Austin Health, Melbourne, Australia

[5] Translational Medicine & Clinical Pharmacology Department, Daiichi-Sankyo Co Ltd, Tokyo, Japan

[6] Biologics Pharmacology Research Laboratories, Daiichi-Sankyo Co Ltd, Tokyo, Japan

[7]Department of Translational Medicine and Clinical Pharmacology, Daiichi-Sankyo Pharma Development, Edison, NJ, USA

[8]Department of Medicine, University of Melbourne, Melbourne, Australia

* - equal contribution

Corresponding Author:

Professor Andrew M. Scott,

Tumour Targeting Laboratory, Olivia Newton-John Cancer Research Institute, 145-163 Studley Road, Heidelberg,

Victoria 3084, Australia

Phone: 61-39496-5876; Fax: 61-39496-5334;

E-mail: andrew.scott@onjcri.org.au

First Authors:

Ingrid Burvenich PhD (Post-doctoral Fellow) and Sagun Parakh MD (PhD student), Tumour Targeting Laboratory, Olivia Newton-John Cancer Research Institute, 145-163 Studley Road, Heidelberg,

Victoria 3084, Australia

Phone: 61-39496-5876; Fax: 61-39496-5334;

Email: sagun.parakh@onjcri.org.au; ingrid.burvenich@onjcri.org.au

Funding: This work was supported by funding from Daiichi-Sankyo Co. Ltd. We acknowledge the Australian Cancer Research Foundation for providing funds to purchase the nanoPET/MR and nanoSPECT/CT imaging equipment and the Operational Infrastructure Support program of the Victorian State Government. This research was also undertaken using the Solid Target Laboratory, an ANSTO-Austin-LICR Partnership.

Conflict of interest: Masakatsu Kotsuma, Jun Hasegawa and Giorgio Senaldi are employees of Daiichi-Sankyo Co. Ltd.

Word Count: **4856**

Short Title: ^{89}Zr-DS-8895a imaging of EphA2 in cancer

ABSTRACT

EphA2 is a cell surface receptor expressed in a range of epithelial cancers. This study evaluated the molecular imaging of EphA2 expression *in vivo* in mouse tumor models using SPECT/MR and PET/MR, utilizing a humanized anti-EphA2 antibody, DS-8895a. **Methods:** DS-8895a was labeled with ^{111}In, ^{125}I and ^{89}Zr, and assessed for radiochemical purity, immunoreactivity (Lindmo analysis), antigen binding affinity (Scatchard analysis) and serum stability *in vitro*. *In vivo* biodistribution, imaging and pharmacokinetic studies were performed, with SPECT/MR and PET/MR imaging undertaken. A dose-escalation study was also performed to determine EphA2 receptor saturability through tissue and imaging quantitative analysis. **Results:** All conjugates demonstrated good serum stability, and specific binding to EphA2 expressing cells *in vitro*. *In vivo* biodistribution studies showed high uptake of ^{111}In-CHX-A″-DTPA-DS-8895a and ^{89}Zr-Df-Bz-NCS-DS-8895a in EphA2 expressing xenograft models, with no specific uptake in normal tissues. In comparison, the retention of ^{125}I-DS-8895a in tumors was lower, due to internalization of the radioconjugate and dehalogenation. These results were confirmed by SPECT/MR and PET/MR imaging. EphA2 receptor saturation was observed at the 30 mg/kg dose level. **Conclusion:** Molecular imaging of tumor uptake of DS-8895a allows non-invasive measurement of EphA2 expression in tumor *in*

vivo, and determination of receptor saturation. ^{89}Zr-Df-Bz-NCS-DS-8895a is suited for human bioimaging trials based on superior imaging characteristics, and will inform DS-8895a dose assessment and patient response evaluation in clinical trials.

Keywords: bioimaging, DS-8895a, EphA2, Zirconium-89, cancer

Introduction

The erythropoietin-producing hepatocellular (Eph) tyrosine kinase receptor group is the largest known family of tyrosine kinase receptors. The receptors consist of an extracellular ligand binding domain, a short transmembrane region and a cytoplasmic kinase domain. There are two subclasses of receptors, EphA (EphA1-10) and EphB (EphB1-6), based on the sequence homologies of the extracellular domain and their binding affinity to glycosylphosphatidylinositol (GPI)-linked ephrin-A (ephrin-A1–5) or transmembrane ephrin-B (ephrin-B1–3) ligands (*1-3*). Activation of the Eph receptor kinase domain can result from a number of processes including binding of ligand to receptor resulting in activation of downstream pathways, contact-dependent cell–cell communication (*2*), and through crosstalk with other signaling systems. Eph/ephrin interactions are particularly important during embryonic development but are also involved in adult tissue homeostasis as they have roles in the development of neuronal pathways, axon guidance formation, maintenance and repair of synaptic junctions, vascular development and epithelial homeostasis (*4-7*).

The EphA2 receptor is strongly overexpressed in a number of cancers including glioblastoma (*8, 9*), ovarian (*10*), prostate adenocarcinoma (*11*), pancreas (*12*), and oesophagus (*13*). Its expression has been associated with

poor prognosis, increased metastasis and decreased survival (*14, 15*). DS-8895a is an afucosylated humanized anti-EphA2 IgG1 monoclonal antibody with enhanced antibody-dependent cellular cytotoxicity (ADCC) expressed using Lonza and BioWa's proprietary POTELLIGENT® CHOK1SV system, showing *in vitro* and anti-tumor efficacy in EphA2 expressing xenograft models.

This study explored the radiolabeling of DS-8895a to iodine-125, and via bifunctional chelates C-functionalized *trans*-cyclohexyldiethylenetriamine-pentaacetic acid (CHX-A″-DTPA) and p-Isothiocyanatobenzyl-desferrioxamine (Df-Bz-NCS) to indium-111 and zirconium-89 respectively, suitable for *in vivo* molecular imaging with SPECT (^{125}I and ^{111}In) and PET (^{89}Zr). The use of such radioconjugates for human bioimaging studies may inform the clinical development of DS-8895a through dose selection and patient response assessment.

MATERIALS AND METHODS

Cell Culture

The human breast carcinoma cell line MDA-MB-231 and human lymphoblastic leukaemia cell line CCRF-CEM were obtained from the American Type Culture Collection (ATCC, Manassas, MD, USA). The cells were cultured in Dulbecco's modified Eagle's medium (DMEM) or RPMI (Invitrogen, Carlsbad, CA, USA) with 10% fetal calf serum and incubated at 37°C with 5% CO_2.

Flow Cytometry

EphA2 expression was assessed by staining 1×10^6 MDA-MB-231 cells with 10 μg/ml of humanized DS-8895a, followed by phycoerythrin anti-human secondary antibody. Flow cytometric analysis was performed using Guava Flow Cytometry (Guava easyCyte 8HT Flow Cytometer; Model: 0500-4008; Massachusetts USA).

Conjugation of Deferoxamine-p-SCN to DS-8895a for radiolabeling

DS-8895a was provided by Daiichi Sankyo Co., Ltd., Tokyo, Japan. It was then chelated with either the bifunctional metal ion chelator, CHX-A"-DTPA (Macrocyclics Inc, Dallas, TX, USA) at 5.0-fold molar excess or Deferoxamine-p-SCN (Df-Bz-NCS; Macrocyclics Inc, Dallas, TX, USA), at 3.0-fold molar excess. Prepared conjugates were aliquoted in 2.0 mg aliquots

prepared in 50 mM sodium acetate buffer (BDH/VWR Chemicals, Australia), pH 5.6, containing 5% w/v sorbitol (BDH/VWR Chemicals, Australia) and 0.01% w/v Tween 80 (Croda, Australia), and stored at -80^{o}C until required.

Radiolabeling and Quality Assurance

Analytical grade reagents, sterile technique and pyrogen-free plasticware were used in all labeling steps. Post chelation, DS-8895a was trace radiolabeled as follows: ^{125}I (Perkin Elmer, Waltham, MA, USA) was attached on tyrosine residues utilizing an Iodogen chemistry (Perkin Elmer); ^{111}In (Mallinckrodt Australia Pty Ltd., Sydney, Australia) on lysine residues via the bifunctional metal ion chelating agent, CHX-A″-DTPA; and ^{89}Zr (PerkinElmer, Melbourne, Australia) on lysine residues via the bifunctional metal ion chelating agent, Df-Bz-NCS. For the two conjugates that utilized chemical chelation (^{111}In-CHX-A″-DTPA-DS-8895a and ^{89}Zr-Df-Bz-NCS-DS-8895a), outcomes of chelation were also assessed. For the former, a solution containing 122 MBq (3.2 mCi) of ^{111}In- (Mallinckrodt Australia Pty Ltd, Sydney, Australia) was mixed with 0.5 mg CHX-A″-DTPA-DS-8895a for 20 minutes. For the latter, a solution containing 44 MBq (1.2 mCi) of ^{89}Zr (PerkinElmer, Melbourne, Australia) was mixed with 1.0 mg Df-Bz-NCS-DS-8895a for 30 minutes. Radiolabeled products were purified on a Sephadex G50 column (Pharmacia, Uppsala, Sweden) equilibrated with sodium chloride injection BP

0.9% w/v (Pfizer, Sydney, Australia). To determine structural integrity post chelation and radiolabeling, constructs were analysed under reducing and non-reducing condition on SDS-PAGE gels. Antibody proteins from CHX-A″-DTPA-DS-8895a, Df-Bz-NCS-DS-8895a and native DS-8895a samples were prepared with and without reducing agents in SDS-PAGE sample buffer. Aliquots of proteins ranging from 1.25 to 5.0 µg were prepared accordingly and analyzed together with known molecular weight markers.

Radiochemical Purity

The amount of free versus bound antibody following radiolabeling was determined by instant thin layer chromatography (ITLC) using silica gel impregnated glass fiber ITLC strips (Gelman Sciences, Inc., Ann Arbor, MI, USA). Assays were performed in duplicate. Radioactivity was measured with an automated gamma counter (Wizard, PerkinElmer, Australia).

Immunoreactivity and Scatchard analysis

The immunoreactive fraction of the radiolabeled DS-8895a constructs with EphA2 positive MDA-MB-231 cells was determined by linear extrapolation to binding at infinite antigen excess using a Lindmo assay as previously described (*16, 17*). Scatchard analysis was used to calculate the apparent association constant (K_a) and number of antibody molecules bound per cell *(16).*

Serum Stability

Serum stability was assessed by incubating 5.0 μg ^{111}In-CHX-A″-DTPA-DS-8895a, 2.5 μg of ^{125}I-DS-8895a and 5.0 μg ^{89}Zr-Df-Bz-NCS-DS-8895a in 100 μL of human serum at 37°C for a 6-day period. Radiochemical purity and single-point immunoreactivity assays at 0 (day of radiolabeling, no incubation), 2 and 6 days of incubation were performed. MDA-MB-231 cells (140×10^6) were used in the single-point binding assays under conditions of antigen excess. Radioconstruct integrity was assessed by Size Exclusion Chromatography (SEC). SEC analyses were performed on a Superdex 200 HR10/30 column at a flow rate of 0.14 mL/min and fraction size of 3.6 mL. The elution buffer was PBS at pH 7.4. Aliquots of serum containing radioconjugates were collected at the specified times and diluted to 1.0 mL using PBS and 10 μL aliquots retained for radioactive counting to determine recovery. The remaining diluted samples of the radioconjugates in serum were loaded onto the column for SEC analysis.

Animal Model

In vivo investigations were performed in 5-6 week old female athymic BALB/c *nu*/*nu* mice (Animal Research Centre, WA, Australia), bearing established EphA2 expressing breast cancer MDA-MB-231 xenografts, or for antigen negative control xenografts, human lymphoblastic leukemia cell line

CCRF-CEM. All animal studies were approved by the Austin Hospital Animal Ethics Committee and were conducted in compliance with the Australian Code for the care and use of animals for scientific purposes. To establish tumors, mice were injected subcutaneously into the left underside flank with EphA2 positive or negative cells (2×10^6 cells) in a total volume of 0.1 mL PBS. Tumor volume (TV) was calculated by the formula [(length × width^2)/2] where length was the longest axis and width the measurement at right angles to length.

Biodistribution Study

In a first biodistribution study, BALB/c *nu*/*nu* mice with established MDA-MB-231 xenografts (TV = 150 – 200 mm^3) received a mixture of 0.185 MBq ^{125}I-DS-8895a (5.0 μg, 5.0 μCi) or 0.6031 MBq ^{111}In-CHX-A″- DTPA-DS-8895a (5.0 μg, 16.3 μCi) intravenously. In a second biodistribution study, BALB/c *nu*/*nu* mice with established MDA-MB-231 (TV range = 207 to 844 mg) or CCRF-CEM xenografts (TV range = 129 to 503 mg) received a dose of 0.1332 MBq ^{89}Zr-Df-Bz-NCS-DS-8895a (5.0 μg, 3.6 μCi) intravenously. On day 0 (2 hours post injection), 1, 2, 3, 5, 7 and 9 or 10 after injection, groups of mice bearing MDA-MB-231 tumors (n = 5) were sacrificed and biodistribution was assessed. For mice bearing EphA2-negative CCRF-CEM xenografts, biodistribution was only assessed at day 2 and 7 post injection.

At the designated time points mice were exsanguinated by cardiac puncture, and tumors and organs [liver, spleen, kidney, muscle, skin, bone (femur), lungs, heart, stomach, brain, small bowel, tail and colon] were collected immediately. All samples were counted in a dual channel gamma scintillation counter (Wizard, PerkinElmer, Australia). Triplicate standards prepared from the injected material were counted at each time point with tissue and tumor samples enabling calculations to be corrected for the physical decay of the isotopes. The tissue distribution data were calculated as the mean ± SD percent injected dose per gram tissue (%ID/g) for the radiolabeled constructs per time point.

Animal Imaging

In order to perform *in vivo* single photon emission computed tomography (SPECT) imaging of ^{111}In-labeled DS-8895a, a separate group of 5 mice received a higher dose of 2.035 MBq (55 μCi) of ^{111}In-CHX-A″- DTPA-DS-8895a (15.7 μg) and were imaged by SPECT, and magnetic resonance (MR) on day 0 (2 hours post injection), 3 and 7 using dedicated small animal nanoSPECT/CT and nanoPET/MR cameras (nanoScan®, Mediso, Budapest, Hungary). In order to perform *in vivo* positron emission tomography (PET) imaging of ^{89}Zr-labeled DS-8895a, a separate group of 5 mice received a dose of 2.775 MBq (75 μCi) of ^{89}Zr-Df-Bz-NCS-DS-8895a (104.2 μg) and were

imaged with PET and MR on day 0 (2 hours post injection), 2 and 7 using a small animal nanoPET/MR camera (nanoScan®, Mediso, Budapest, Hungary).

Pharmacokinetics

Serum from blood collected from tumor-bearing mice injected with radiolabeled antibody was aliquoted and counted in a gamma counter (Packard). Triplicate standards prepared from the injected material were also counted at each time point to enable calculations to be corrected for the isotope physical decay. The results of the serum were expressed as % injected dose per litre (%ID/L) and the serum concentrations (μg/mL) calculated. A two compartment IV bolus model with macro-parameters, no lag time and first order elimination (WNL Model 8) was fitted to serum data for each animal using un-weighted non-linear, least squares with Phoenix WinNonLin (Certara, St Louis, MO). Estimates were determined for the pharmacokinetic parameters: $t_{½\alpha}$ and $t_{½\beta}$ (half-lives of the initial and terminal phases of disposition); Vss (volume at steady state); Cmax (maximum serum concentration); AUC (area under the serum concentration curve extrapolated to infinite time); and CL (total serum clearance).

EphA2 Saturation *In Vivo*

The influence of DS-8895a protein dose on tumor uptake and EphA2 saturation *in vivo* was determined in a separate biodistribution and PET/MR

imaging study using ^{89}Zr-Df-Bz-NCS-DS-8895a. For the biodistribution study, three groups of mice (n = 5) were injected with 0.2775 MBq ^{89}Zr-Df-Bz-NCS-DS-8895a (5.5 μg, 7.5 μCi) combined with different amounts of unlabeled DS-8895a to achieve a total protein dose of 0.3, 3, and 30 mg/kg in a total volume of 0.1 mL 0.9% w/v of NaCl. At day 2 and day 7 after injection, all animals were sacrificed and organs were collected as described above. The tissue distribution data was calculated as the mean ± SD %ID/g.

In parallel, 1-2 mice of each group were imaged at day 0 (2 hours post injection), 2 and 7 post injection using the small animal nanoPET/MR camera (nanoScan®, Mediso, Budapest, Hungary) as described before. Imaging analysis was performed on the series of PET/MR images acquired. Tumor uptake (kBq/cc) was determined by mark-up of volumes of interest (VOI) in cross-sectional PET images. Tumor volume (mL) was determined based on mark-up of VOI in cross-sectional MR images. To convert (kBq/cc)/mL to %ID/mL, total body uptake (kBq/cc) in mice was measured at day 0 as an approximation of injected dose (ID).

Statistical Analysis

A paired t-test was used to determine significant differences between tissues (%ID/g) of ^{89}Zr-biodistribution results. An unpaired t-test was used to determine significant differences of pharmacokinetic parameters calculated for

^{111}In- and ^{89}Zr-labeled DS-8895a antibody. For multiple comparisons, one-way ANOVA was used. All analyses were done using Graphpad Prism version 6.03. Data are presented as the average ± SD, unless stated differently.

RESULTS

Conjugation, Radiolabeling and Quality Assurance

The results of chelation and radiolabeling were assessed using MDA-MB-231 cells, which were confirmed to have high EphA2 expression. All three radioconjugates were intact by SDS-PAGE analysis under reducing and non-reducing conditions (data not shown). Data was also obtained for stability of ^{111}In-CHX-A″-DTPA-DS-8895 (purity, 91.2%; immunoreactivity, 44.0%), ^{125}I-DS-8895a (purity, 94.5%; immunoreactivity, 46.6%) and ^{89}Zr-Df-Bz-NCS-DS-8895a (purity, 97.5%; immunoreactivity, 51%) at 6 days in human serum.

Using a Lindmo binding assay with MDA-MB-231 cells, the ^{125}I-DS-8895a chelate showed 98.9% radiochemical purity, immunoreactivity of 53.8% and apparent K_a of 2.14 x 10^8 M^{-1} (Fig. 1A). The ^{111}In-CHX-A″-DTPA-DS-8895 chelate showed high purity (99.6%), immunoreactivity of 55.4% and apparent K_a of 2.10 x 10^8 M^{-1} (Fig. 1B). ^{89}Zr-Df-Bz-NCS-DS-8895a had a radiochemical purity of 99.6% and immunoreactivity of 54.2% (Fig. 1C). Scatchard analysis indicated that the ^{111}In-conjugate bound to approximately 40,000 sites per cell (Fig. 1D) compared with 60,000 antibodies binding sites per cell for both ^{125}I-DS-8895a and ^{89}Zr-Df-Bz-NCS-DS-8895a (Fig. 1E and 1F).

Biodistribution

Figure 2 summarizes the biodistribution results of ^{125}I-DS-8895a, ^{111}In-CHX-A″-DTPA-DS-8895a and ^{89}Zr-Df-Bz-NCS-DS-8895a in EphA2 positive MDA-MB-231 tumors. ^{125}I-DS-8895a tumor uptake was lowest, reaching only 11.23 ± 4.34 %ID/g by day 2 post injection and declined to 3.42 ± 0.73 %ID/g tumor by day 10. In comparison, the uptake of ^{111}In-CHX-A″-DTPA-DS-8895a reached a maximum of 23.19 ± 12.17 %ID/g on day 2 post injection and gradually declined to 8.76 ± 3.65 %ID/g by day 10 post injection. The uptake of ^{89}Zr-Df-Bz-NCS-DS-8895a reached a level of 26.59 ± 3.04 %ID/g on day 3 post injection, maintaining this level of 28.24 ± 3.66 %ID/g at day 5 before gradually declining to 20.82 ± 4.67 %ID/g by day 9 post injection.

Organs with high blood supply including heart, kidneys, liver, spleen and lungs, showed high initial uptake of radiolabeled DS-8895a (Fig. 2) consistent with biodistribution and catabolism of radiolabeled antibodies. Uptake of radioiodinated DS-8895a in these organs declined over time. In contrast, uptake in spleen, liver and bone remained high or increased over time with the ^{111}In- and ^{89}Zr-conjugates, consistent with catabolism of radiometal conjugated antibodies (Fig. 2).

The tumor-to-blood ratio for ^{125}I-DS-8895a increased from 0.23 (2 hours post injection) to 0.33 (day 7 post injection). In comparison, the tumor-to-blood ratio for ^{111}In-CHX-A″-DTPA-DS-8895a increased from 0.17 (2 hours

post injection) to 0.94 (day 7 post injection) and the tumor-to-blood ratio for ^{89}Zr-Df-Bz-NCS-DS-8895a increased from 0.14 (day 0 (2 hours post injection)) to 3.62 (day 7 post injection). The tumor specificity of ^{89}Zr-Df-Bz-NCS-DS-8895a was confirmed by assessing uptake in the EphA2 negative tumor CCRF-CEM (Fig. 3). Tumor uptake of ^{89}Zr-Df-Bz-NCS-DS-8895a in CCRF-CEM tumors at day 2 post injection was significantly lower than MDA-MB-231 (7.58 ± 0.29 %ID/g versus 21.52 ± 2.65 respectively; $P = 8.40 \times 10^{-6}$), and also at day 7 post injection (6.73 ± 1.21 %ID/g versus 23.64 ± 4.06 respectively; $P = 4.43 \times 10^{-5}$).

***In vivo* molecular imaging of EphA2 expression in tumor**

Whole body SPECT/MR images showed localization of ^{111}In-CHX-A″-DTPA-DS-8895a to tumors at early time points post injection (from 2 hours) (Fig. 4A). ^{111}In-CHX-A″-DTPA-DS-8895a uptake in tumors was more discernible at later time points up to 7 days, even in the small sized tumors.

Similarly, whole body PET/MR images showed localization of ^{89}Zr-Df-Bz-NCS-DS-8895a (Fig. 4B) to tumors at early time points post injection (from 2 hours). ^{89}Zr-Df-Bz-NCS-DS-8895a uptake in tumors was also clearly discernible at later time points, up to 7 days post injection, even in the small sized tumors. Some spleen and liver activity, and bone uptake, consistent with catabolism of ^{89}Zr-Df-Bz-NCS, was also observed.

***In vivo* receptor saturation**

A combination study of biodistribution and PET/MR imaging explored the saturation of the EphA2 receptor *in vivo*. A biodistribution study compared 0.3, 3 and 30 mg/kg dose of ^{89}Zr-labeled DS-8895a in mice bearing MDA-MB-231 xenografts (TV = 0.647 ± 0.194 g). No significant differences were observed in blood and normal tissue biodistribution patterns (data not shown).

A clear protein dose effect was evident for MDA-MB-231 tumor uptake. At all study time points, highest tumor uptake was observed at the 0.3 mg/kg DS-8895a dose, and lowest tumor uptake at 30 mg/kg, and significantly higher tumor-to-blood ratios were observed at 0.3 mg/kg protein dose compared to the 30 mg/kg dose over the duration of the study (Fig. 5). No significant differences in average tumor size of each dose level group were observed indicating that the protein dose effect was not influenced by tumor size in the study.

Representative individual animal PET/MR images of 0.3, 3 and 30 mg/kg ^{89}Zr-labeled DS-8895a at day 2 and 7 are shown in Figure 6. MDA-MB-231 tumor uptake was clearly evident at day 2 (Fig. 6A) and day 7 (Fig. 6B) at all dose levels. Compared to the 0.3 mg/kg dose level, both the 3 and the 30 mg/kg DS-8895a dose levels showed less uptake in the MDA-MB-231 xenografts with time, consistent with the measured %ID/g levels and tumor-to-

blood ratios as obtained from the biodistribution study (Fig. 5). Quantitative image analysis of tumor volumes and tumor uptake confirmed a substantial reduction of tumor uptake at both 3.0 mg/kg and 30 mg/kg dose levels (data not shown).

Pharmacokinetics

The mean pharmacokinetic parameters for ^{111}In- and ^{89}Zr-labeled DS-8895a administered at protein doses of 5 μg (0.25 mg/kg) are presented in Table 1. An unpaired t-test determined significant differences in the pharmacokinetic parameters between the two radioconjugates. The slightly faster clearance observed with the ^{89}Zr-labeled DS-8895a is consistent with the higher tumor uptake observed with this radioconjugate.

DISCUSSION

We have shown that it is feasible to radiolabel DS-8895a, an anti-EphA2 antibody, with a number of radioligands suitable for SPECT (^{125}I and ^{111}In) and PET (^{89}Zr) molecular imaging. Chelation and radiolabeling did not alter the structural integrity or immunoreactivity of the constructs. These constructs were also stable in plasma for up to 6 days.

The *in vivo* biodistribution and imaging patterns showed that ^{125}I-DS-8895a had the lowest tumor uptake of all the conjugates at all time points tested. This likely reflects internalization and translocation of ^{125}I-DS-8895a to the lysosomes with subsequent degradation of the conjugate and release of the ^{125}I-catabolites out of the cells. In contrast, ^{111}In- and ^{89}Zr-catabolites are trapped in the cell, allowing higher retention of ^{111}In- and ^{89}Zr-conjugates in the xenografts.

The *in vivo* targeting of tumor with ^{111}In-CHX-A″-DTPA- and ^{89}Zr-Df-Bz-NCS-DS-8895a was similar, although the latter was higher particularly at later time points. The results for ^{89}Zr- Df-Bz-NCS-DS-8895a are superior to a prior study of anti-EphA2 ^{64}Cu-DOTA-1C1, particularly at later time points, where maximal uptake in human tumors is anticipated and where ^{89}Zr half-life is better suited to human trials (*18*). These results are also comparable to uptake of other ^{89}Zr-labeled antibodies in animal models, including Herceptin®,

although it is worth emphasizing that the expression of ErbB2 on tumor cell surface is much higher than EphA2 (*19-22*).

The impact of protein dose on EphA2 targeting and receptor saturation *in vivo* has not previously been assessed, and reduced tumor uptake of ^{89}Zr-Df-Bz-NCS-DS-8895a was observed at the 3.0 mg/kg dose level, with slightly lower uptake at 30 mg/kg dose level. The 3 mg/kg dose level is within the likely dose range for clinical trials, indicating that EphA2 receptor saturation may occur during dose escalation, thus justifying a bioimaging approach to dose assessment in early phase trials (*23*).

Overall, we have developed three radiolabeled conjugates for DS-8895a, and ^{89}Zr-Df-Bz-NCS-DS-8895a is our lead compound because of its superior imaging and tumor uptake characteristics. There is direct clinical relevance of these findings as we have previously shown in several first-in-man clinical bioimaging studies that there is an excellent correlation between preclinical and clinical biodistribution data and gamma camera imaging using radiolabeled monoclonal antibodies (*24-27*).

CONCLUSION

We have shown that molecular imaging of radiolabeled DS-8895a allows non-invasive quantitative assessment of EphA2 expression, and receptor saturation,

in tumor models. These results have direct relevance to the design and conduct of DS-8895a clinical trials in cancer patients, and a clinical trial of ^{89}Zr-Df-Bz-NCS-DS-8895a in patients with EphA2 expressing tumors is underway.

DISCLOSURE

Masakatsu Kotsuma, Jun Hasegawa and Giorgio Senaldi are employees of Daiichi-Sankyo Co. Ltd. This work was supported by funding from Daiichi-Sankyo Co. Ltd. We acknowledge the Australian Cancer Research Foundation for providing funds to purchase the PET/MR and nanoSPECT/CT imaging equipment and the Operational Infrastructure Support program of the Victorian State Government. This research was also undertaken using the Solid Target Laboratory, an ANSTO-Austin-LICR Partnership.

REFERENCES

1. Gale NW, Yancopoulos GD. Ephrins and their receptors: a repulsive topic? *Cell Tissue Res.* 1997;290:227-241.

2. Kullander K, Klein R. Mechanisms and functions of Eph and ephrin signalling. *Nat Rev Mol Cell Biol.* 2002;3:475-486.

3. Murai KK, Pasquale EB. 'Eph'ective signaling: forward, reverse and crosstalk. *J Cell Sci.* 2003;116:2823-2832.

4. Pasquale EB. Eph-ephrin bidirectional signaling in physiology and disease. *Cell.* 2008;133:38-52.

5. Flanagan JG, Vanderhaeghen P. The ephrins and Eph receptors in neural development. *Annu Rev Neurosci.* 1998;21:309-345.

6. Yamaguchi Y, Pasquale EB. Eph receptors in the adult brain. *Curr Opin Neurobiol.* 2004;14:288-296.

7. Hafner C, Schmitz G, Meyer S, et al. Differential gene expression of Eph receptors and ephrins in benign human tissues and cancers. *Clin Chem.* 2004;50:490-499.

8. Wykosky J, Gibo DM, Stanton C, Debinski W. Interleukin-13 receptor alpha 2, EphA2, and Fos-related antigen 1 as molecular denominators of high-grade astrocytomas and specific targets for combinatorial therapy. *Clin Cancer Res.* 2008;14:199-208.

9. Wang LF, Fokas E, Bieker M, et al. Increased expression of EphA2 correlates with adverse outcome in primary and recurrent glioblastoma multiforme patients. *Oncol Rep.* 2008;19:151-156.

10. Thaker PH, Deavers M, Celestino J, et al. EphA2 expression is associated with aggressive features in ovarian carcinoma. *Clin Cancer Res.* 2004;10:5145-5150.

11. Zeng G, Hu Z, Kinch MS, et al. High-level expression of EphA2 receptor tyrosine kinase in prostatic intraepithelial neoplasia. *Am J Pathol.* 2003;163:2271-2276.

12. Duxbury MS, Ito H, Zinner MJ, Ashley SW, Whang EE. EphA2: a determinant of malignant cellular behavior and a potential therapeutic target in pancreatic adenocarcinoma. *Oncogene.* 2004;23:1448-1456.

13. Miyazaki T, Kato H, Fukuchi M, Nakajima M, Kuwano H. EphA2 overexpression correlates with poor prognosis in esophageal squamous cell carcinoma. *Int J Cancer.* 2003;103:657-663.

14. Liu F, Park PJ, Lai W, et al. A genome-wide screen reveals functional gene clusters in the cancer genome and identifies EphA2 as a mitogen in glioblastoma. *Cancer Res.* 2006;66:10815-10823.

15. Kinch MS, Moore MB, Harpole DH, Jr. Predictive value of the EphA2 receptor tyrosine kinase in lung cancer recurrence and survival. *Clin Cancer Res.* 2003;9:613-618.

16. Lindmo T, Boven E, Cuttitta F, Fedorko J, Bunn PA, Jr. Determination of the immunoreactive fraction of radiolabeled monoclonal antibodies by linear extrapolation to binding at infinite antigen excess. *J Immunol Methods.* 1984;72:77-89.

17. Lee FT, Rigopoulos A, Hall C, et al. Specific localization, gamma camera imaging, and intracellular trafficking of radiolabelled chimeric anti-G(D3) ganglioside monoclonal antibody KM871 in SK-MEL-28 melanoma xenografts. *Cancer Res.* 2001;61:4474-4482.

18. Cai W, Ebrahimnejad A, Chen K, et al. Quantitative radioimmunoPET imaging of EphA2 in tumor-bearing mice. *Eur J Nucl Med Mol Imaging.* 2007;34:2024-2036.

19. Dijkers EC, Kosterink JG, Rademaker AP, et al. Development and characterization of clinical-grade 89Zr-trastuzumab for HER2/neu immunoPET imaging. *J Nucl Med.* 2009;50:974-981.

20. Janjigian YY, Viola-Villegas N, Holland JP, et al. Monitoring afatinib treatment in HER2-positive gastric cancer with 18F-FDG and 89Zr-trastuzumab PET. *J Nucl Med.* 2013;54:936-943.

21. Holland JP, Divilov V, Bander NH, Smith-Jones PM, Larson SM, Lewis JS. 89Zr-DFO-J591 for immunoPET of prostate-specific membrane antigen expression in vivo. *J Nucl Med.* 2010;51:1293-1300.

22. Deri MA, Zeglis BM, Francesconi LC, Lewis JS. PET imaging with (8)(9)Zr: from radiochemistry to the clinic. *Nucl Med Biol.* 2013;40:3-14.

23. Burvenich IJ, Lee FT, Cartwright GA, et al. Molecular imaging of death receptor 5 occupancy and saturation kinetics in vivo by humanized monoclonal antibody CS-1008. *Clin Cancer Res.* 2013;19:5984-5993.

24. Scott AM, Lee FT, Tebbutt N, et al. A phase I clinical trial with monoclonal antibody ch806 targeting transitional state and mutant epidermal growth factor receptors. *Proc Natl Acad Sci U S A.* 2007;104:4071-4076.

25. Scott AM, Lee FT, Jones R, et al. A phase I trial of humanized monoclonal antibody A33 in patients with colorectal carcinoma: biodistribution, pharmacokinetics, and quantitative tumor uptake. *Clin Cancer Res.* 2005;11:4810-4817.

26. Herbertson RA, Tebbutt NC, Lee FT, et al. Phase I biodistribution and pharmacokinetic study of Lewis Y-targeting immunoconjugate CMD-193 in patients with advanced epithelial cancers. *Clin Cancer Res.* 2009;15:6709-6715.

27. Herbertson RA, Tebbutt NC, Lee FT, et al. Targeted chemoradiation in metastatic colorectal cancer: a phase I trial of 131I-huA33 with concurrent capecitabine. *J Nucl Med.* 2014;55:534-539.

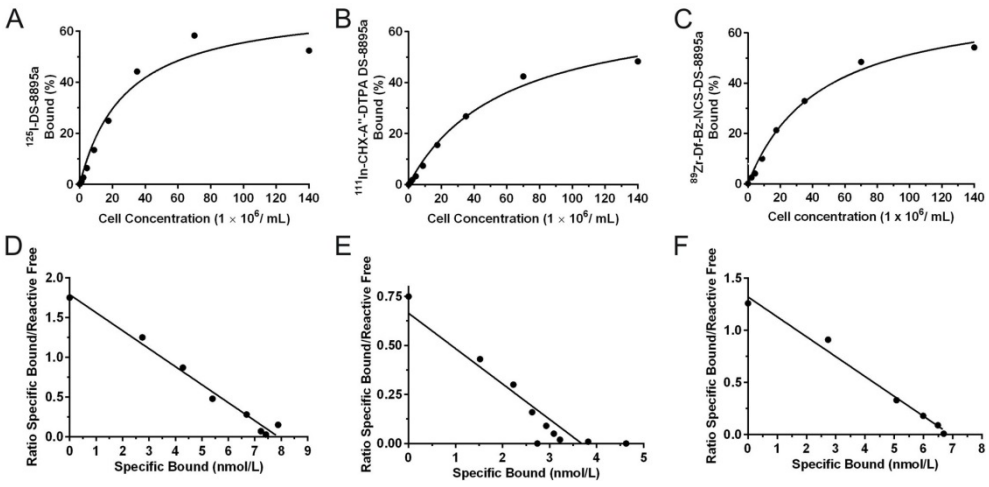

FIGURE 1. *In vitro* binding assays with radiolabeled DS-8895a. Lindmo plots showing binding of (A) ^{125}I-DS-8895a, (B) ^{111}In-CHX-A″-DTPA-DS-8895a and (C) ^{89}Zr-Df-Bz-NCS-DS-8895a to increasing concentrations of EphA2 positive MDA-MB-231 cells. Scatchard plot of (D) ^{125}I-DS-8895a, (E) ^{111}In-CHX-A″-DTPA-DS-8895a and (F) ^{89}Zr-Df-Bz-NCS-DS-8895a binding to MDA-MB-231 cells.

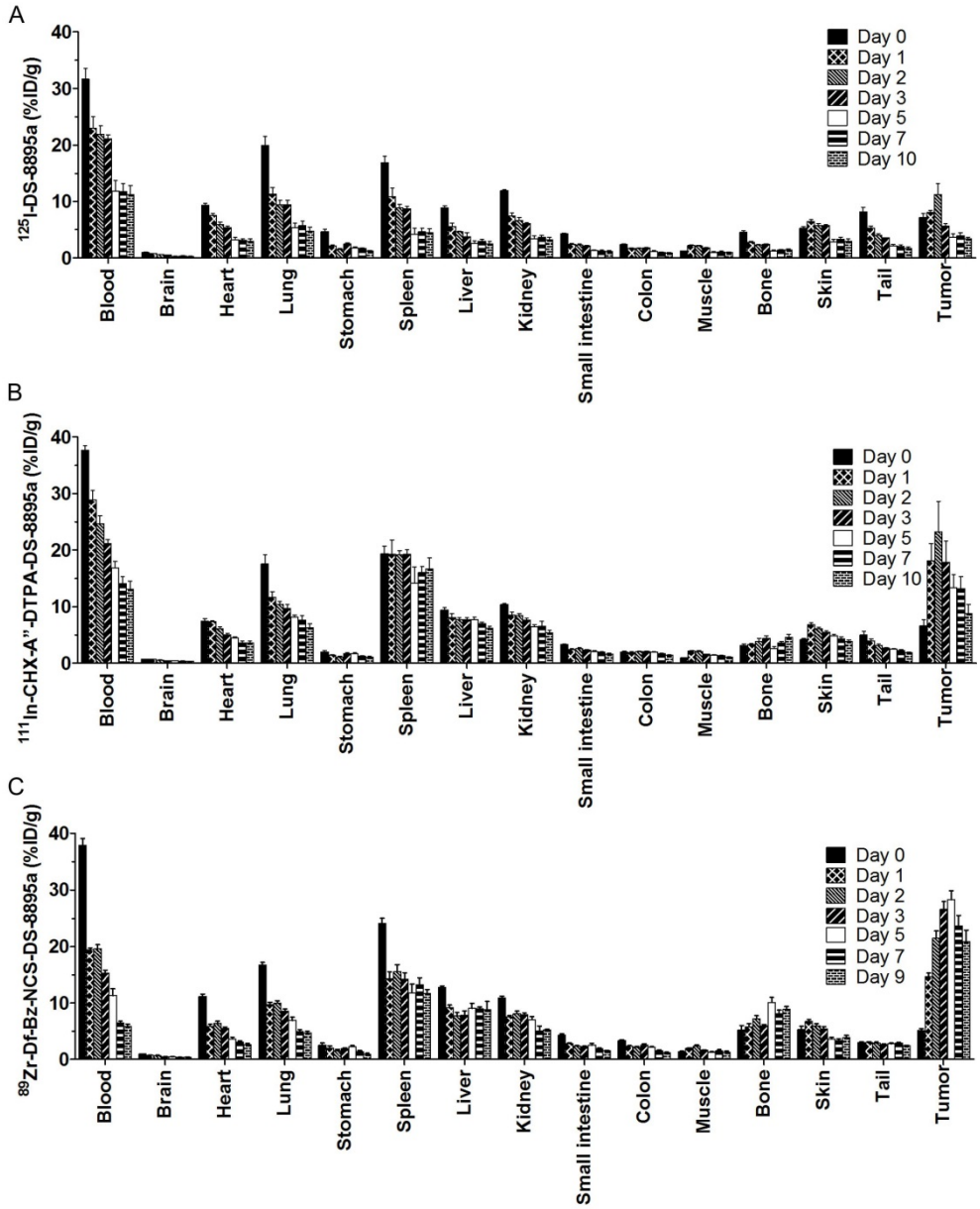

FIGURE 2. Biodistribution properties of (A) ^{125}I-DS-8895a, (B) ^{111}In-CHX-A″-DTPA-DS-8895a and (C) ^{89}Zr-Df-Bz-NCS-DS-8895a in MDA-MB-231 xenografted BALB/c *nu*/*nu* mice. *Bars*, mean ± SD; $n = 5$

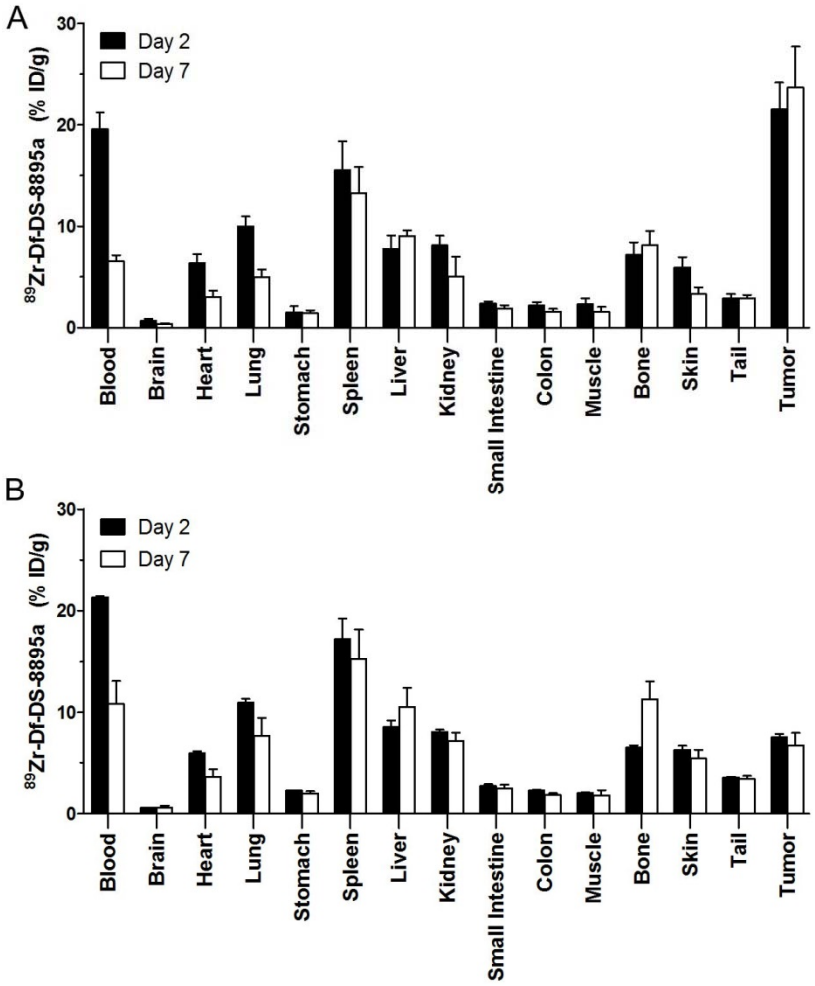

FIGURE 3. Biodistribution properties of ^{89}Zr-Df-Bz-NCS-DS-8895a in BALB/c *nu*/*nu* mice bearing (A) EphA2-positive MDA-MB-231 breast tumors and (B) EphA2-negative CCRF-CEM human lymphoblastic leukaemia at day 2 and 7 post injection. *Bars*, mean ± SD; $n = 5$

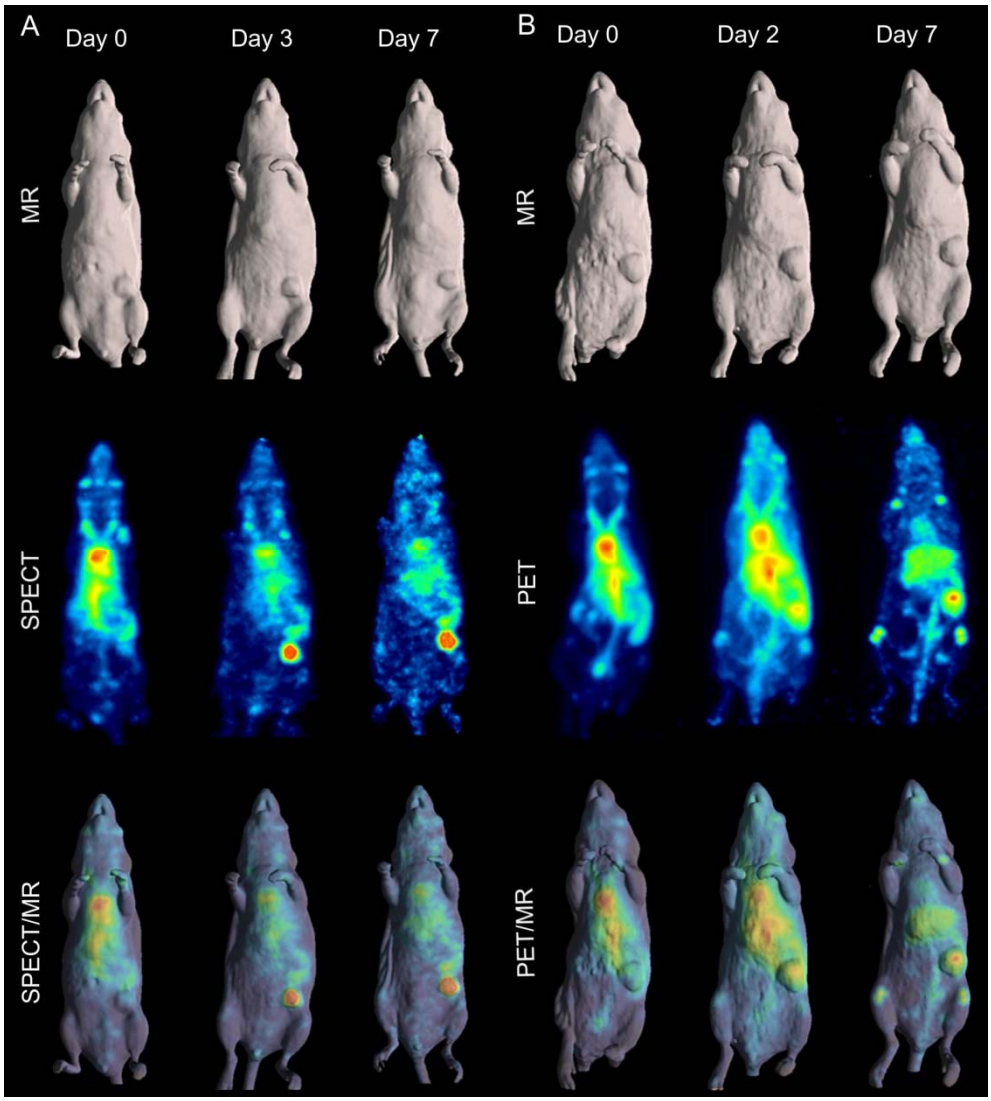

FIGURE 4. (A) MR (surface rendered, *top row*), SPECT (maximum intensity projection, *middle row*) and fused SPECT/MR (*bottom row*) images of MDA-MB-231 xenografted mice taken at day 0 (2 hours post injection), 3 and 7 post injection of ^{111}In-CHX-A″-DTPA-DS-8895a. (B) MR (surface rendered, *top row*), PET (maximum intensity projection, *middle row*) and fused PET/MR (*bottom row*) images of MDA-MB-231 xenografted mice taken at day 0 (2 hours post injection), 2 and 7 post injection of ^{89}Zr-Df-Bz-NCS-DS-8895a.

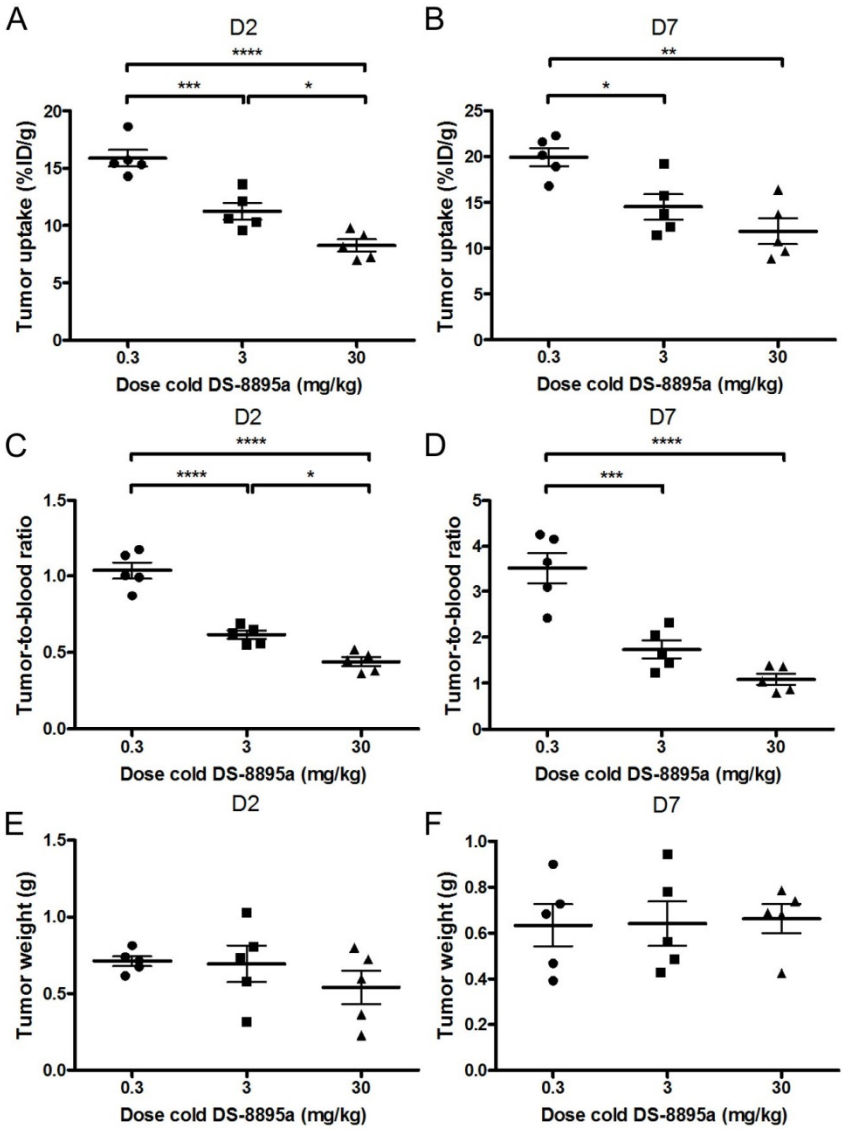

FIGURE 5. Influence of cold dose DS-8895a on tumor uptake of ^{89}Zr-Df-Bz-NCS-DS-8895a in BALB/c *nu*/*nu* mice bearing MDA-MB-231 xenografts (A) at day 2 and (B) at day 7 post injection, and tumor-to-blood ratios (C) at day 2 and (D) at day 7 post injection. No significant differences were observed between average tumor sizes of each dose level (E) at day 2 and (F) at day 7 post injection. *Bars*, SEM; $n = 5$. *, $P < 0.05$; **, $P < 0.005$; ***, $P < 0.0005$; ****, $P < 0.0001$

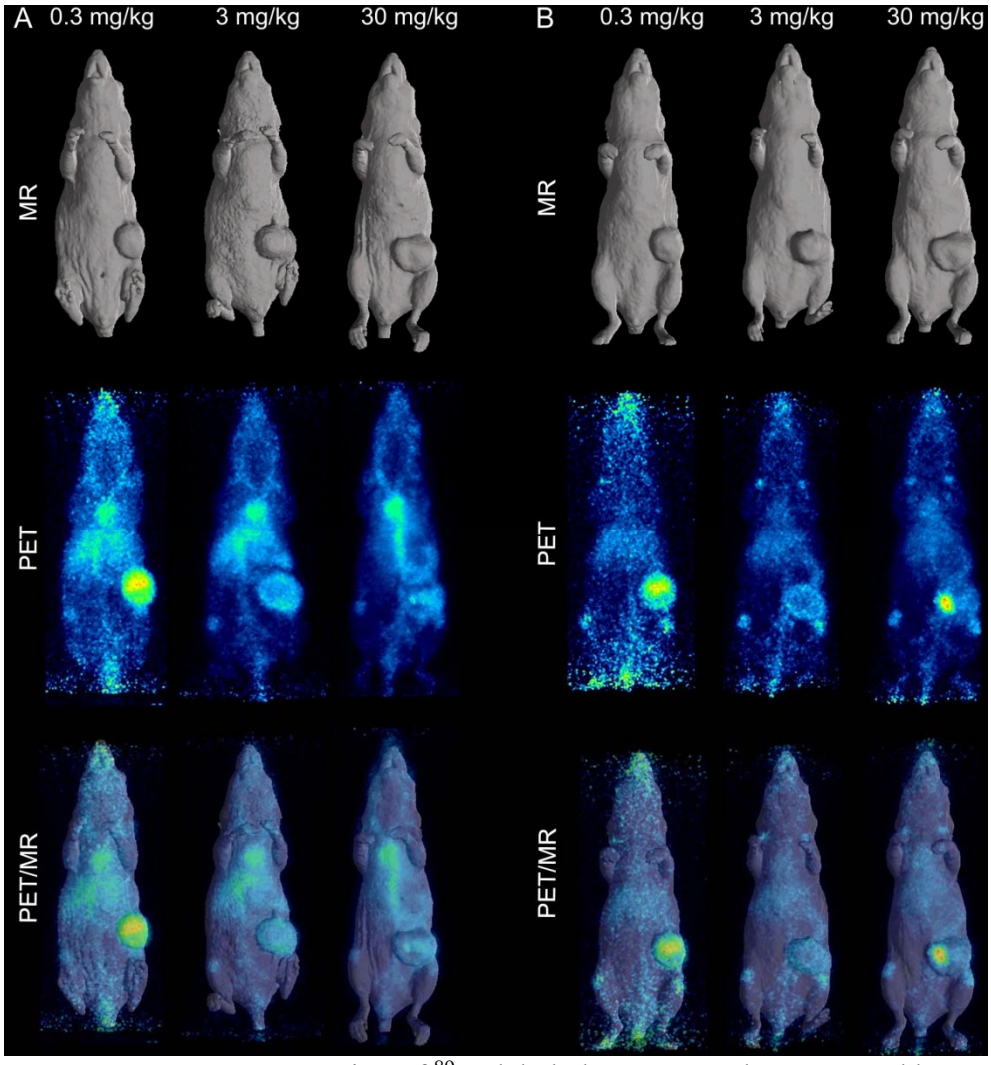

FIGURE 6. *In vivo* saturation of ^{89}Zr-labeled DS-8895a demonstrated by PET/MR (A) at day 2 and (B) at day 7 post injection. Representative whole body surface-rendered MR images (*top*), maximum intensity projection PET image (*middle*) and fused PET/MR images (*bottom*) are shown for each time point at different dose levels of cold DS-8895a (0.3, 3 and 30 mg/kg). The hot spot in the tumor visible in the PET and PET/MR images of the mouse receiving the 30 mg/kg dose at day 7 post injection is due to the presence of a blood crust.

TABLE 1 Pharmacokinetic parameters of ^{89}Zr- and ^{111}In-labeled DS-8895a in MDA-MB-231 tumor-bearing mice

Parameters	**^{89}Zr-labeled DS-8895a**[*]	**^{111}In-labeled DS-8895a**	***P*-value**[†]
AUC (h × μg/mL)	185.7 ± 26.96	417.6 ± 90.60	0.0033
$t_{½\,\alpha}$ (h)	1.48 ± 0.26	8.85 ± 4.97	0.0295
$t_{½\,\beta}$ (h)	102.4 ± 14.65	215.1 ± 72.88	0.0244
Cmax (μg/mL)	3.03 ± 0.43	2.07 ± 0.29	0.0033
C_L (mL/h)	0.027 ± 0.004	0.012 ± 0.002	< 0.0001
V_{ss} (mL)	3.90 ± 0.11	3.59 ± 0.43	0.1845 (*ns*)

Abbreviations: AUC, area under the curve; $t_{½\,\alpha}$, half-life of initial phase disposition; $t_{½\,\beta}$ half-life of the terminal phase of disposition; C_{max}, maximum plasma-serum concentration; C_L, total serum clearance; V_{ss}, volume of distribution at steady state; *ns*, not significantly different

[*]Data presented as mean ± SD (n = 5); [†], Results of an unpaired t-test, Welch's correction was used when variances were significantly different